Angular Distribution of Protons from Collisional Dissociation of H_2^+. II. Vibrational Dissociation*

Thomas A. Green
Sandia Laboratories, Albuquerque, New Mexico 87115
(Received 1 December 1969)

A classical-impulse binary-collision model is used to predict the laboratory angle and velocity distributions of protons resulting from the vibrational dissociation of H_2^+ by He. The treatment is partly heuristic and is not a quantitative success, since the computed cross sections turn out to be roughly an order of magnitude too large compared to those for electronic excitation of the $2p\sigma_u$ state of H_2^+. Nonetheless, the theory clearly identifies some major features of the experimental results of Gibson, Los, and Schopman as being due to vibrational dissociation.

I. INTRODUCTION

The object of this work is to show that vibrational dissociation accounts for some salient features of the angle and velocity distributions of protons resulting from collisions of fast H_2^+ with neutral target atoms. Since the classical-impulse binary collision model, upon which the work is based, is used at impact velocities below its realm of quantitative validity, the results are qualitative in nature. The results are nonetheless convincing as regards identification of the dissociation mechanism. In addition, the calculations show what aspects of the mechanics of vibrational dissociation are likely to be important in the development of a quantitative theory. Figure 1, reproduced from the work of Gibson, Los, and Schopman,[1] exemplifies the experimental data which motivated the work. The curves represent proton angle and velocity distributions obtained from laboratory frame measurements but transformed to a frame based on the H_2^+ c.m. Each curve corresponds to a fixed c.m. dissociation velocity and is labeled by the internuclear separation required by the assumption that the dissociation occurs via a vertical transition from the initial $1s\sigma_g$ electronic state to the nominally repulsive $2p\sigma_u$ state. Aside from the vicinity of c.m. dissociation angle $\phi = 90°$, the distributions agree qualitatively with theoretical c.m. angular distributions for $2p\sigma_u$ excitation.[1] However, the central portions of the curves, particularly the peak in the curve for $R = 2.4\ a_0$, do not resemble the angular distributions to be expected for any of the probable electronic excitations of H_2^+.[2] It will be shown that vibrational dissociation explains the discrepancy qualitatively in a natural way.

The calculations are based on a classical-impulse binary collision model, closely related to models previously used for the estimation of total vibrational dissociation cross sections.[3–5] In this model, dissociation yielding a proton with speed u relative to the H_2^+ c.m. occurs when one or the other of the H_2^+ protons experiences an impulsive momentum change of magnitude K, related to u through internal energy conservation by

$$\tfrac{1}{2}K^2/2m = mu^2 + D_\nu \ , \qquad (1)$$

where m is the proton mass and D_ν is the dissociation energy of the initial vibrational state ν. Since $D_\nu \sim 0.1$ a.u. for the lower values of ν, vibrational dissociation of these states involves large values of K ($K \gtrsim 20$ a.u.). Because of the momentum change $\vec{K}$, the H_2^+ c.m. is deflected through an angle $\sim K/(2mV_0)$ where V_0 is the initial H_2^+ speed. Deflections ~ 1 deg are not unlikely. Since the laboratory measurements are made for angles between 0° and about 2°, the H_2^+ c.m. deflection can play an important role in determining at what laboratory angle the dissociation proton is likely to emerge.

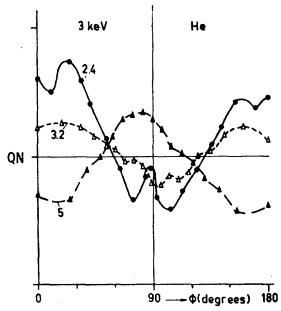

FIG. 1. Apparent c.m. angular dependence of the dissociation of 3-keV H_2^+ ions incident on He. The ordinate QN is normalized so that $\frac{1}{2}\int_0^\pi \sin\phi\, QN\, d\phi = 1$. The angle ϕ is measured from the backward beam direction.

The other essential features of the calculation are the screening of the bare nuclei by the electrons in the system, and the correlation between $\vec{K}$ and the c.m. dissociation velocity $\vec{u}$. For small values of K, the former drastically influences the probability that the momentum change $\vec{K}$ will occur in a given collision. The latter, treated heuristically in this paper, determines the dissociation angular distribution in the H_2^+ frame and consequently has a considerable quantitative influence on the proton angle and velocity distributions in the laboratory frame.

The details and limitations of the model are discussed in Sec. II. Results relating to Fig. 1, and other results illustrating the essential features of the model, are given in Sec. III. The model will be applied to other H_2^+ dissociation experiments[6-8] in the third paper of this series.

II. THEORY

Although the final results are essentially classical, it is instructive to obtain them starting from the Born approximation. The H_2^+ projectile is assumed to be initially nonrotating in the νth vibrational level of its ground electronic state and to dissociate during a collision with some target atom. In a.u., the cross section Q_ν for vibrational dissociation is then

$$Q_\nu = 4V_0^{-2}\int_0^{k_{\max}} k^2\,dk \int d\Omega(\hat{k}) \int_{k_0-k_n}^{k_0+k_n} dK K^{-3}|\epsilon_T|^2 \times \int_0^{2\pi} d\phi_K \left|E_g(-\vec{K},\vec{k})\right|^2 . \quad (2)$$

In Eq. (2), $\vec{k}=m\vec{u}$, where m is the proton mass and $\vec{u}$ is the proton velocity relative to the H_2^+ c.m. after dissociation: $\vec{K}$ is the momentum transferred to the target and ϕ_K is its azimuthal angle in the laboratory frame; $k_0=\mu V_0$ and $k_n=\mu V_n$, where μ is the H_2^+-target reduced mass, and V_0 and V_n are the relative speeds before and after collision; $k_{\max}$ is the largest value of k allowed by energy conservation. The quantity $|\epsilon_T|^2$ describes the transition in the target and is expressed in terms of the target's coherent or incoherent x-ray scattering factor.[9]

Finally, $E_g(\vec{K},\vec{k}) = J(\vec{K},\vec{k}) - I(\vec{K},\vec{k}) - I(-\vec{K},\vec{k})$, (3)

where
$$I(\vec{K},\vec{k}) = \int d\vec{R}\chi^*\, e^{i\vec{K}\cdot\vec{R}/2}\chi_\nu ,$$
$$J(\vec{K},\vec{k}) = \int d\vec{R}\chi^*\chi_\nu \int d\vec{r}\,\phi_0^* e^{i\vec{K}\cdot\vec{r}}\phi_0 . \quad (4)$$

Here $\vec{R}$ is the H_2^+ internuclear separation, $\vec{r}$ locates the H_2^+ electron with respect to the center of the internuclear line, and ϕ_0 is the $1s\sigma_g$ electronic wave function; χ_ν and χ are the initial and final H_2^+ vibration-rotation wave functions. Equations (2)–(4) result from a straightforward application of the Born approximation. They may be deduced from Eqs. (1), (2), (8), and (10) of Ref. 2.

The matrix element $E_g(\vec{K},\vec{k})$ will now be considerably simplified through the use of additional approximations. First ϕ_0 is replaced by its linear combination of atomic orbitals (LCAO) approximation, and the multicenter terms which arise in the evaluation of $J(\vec{K},\vec{k})$ are neglected. This leads to

$$E_g(\vec{K},\vec{k}) = -\left[1-\tfrac{1}{2}(1+\tfrac{1}{4}K^2)^{-2}\right]\left[I(\vec{K},\vec{k})+I(-\vec{K},\vec{k})\right] . \quad (5)$$

To motivate this approximation we note that for low ν (small R) large values of K are required for dissociation. Consequently $J(\vec{K},\vec{k}) \ll I(\vec{K},\vec{k})$ and the fact that $J(\vec{K},\vec{k})$ is not accurate is unimportant. For large ν, where K need not be large, large values of R dominate $J(\vec{K},\vec{k})$ and the approximation is reasonable.[10]

The next approximation is to neglect the cross terms $I(\vec{K},\vec{k})I(-\vec{K},\vec{k})^*$, etc., which arise in $|E_g(\vec{K},\vec{k})|^2$. This reduces the theory to a binary collision theory of the form studied by Gerasimenko and Oksyuk,[11] who developed their formulas by adding up the probabilities for dissociation via impulsive momentum transfer to just one or just the other of the nuclei of a diatomic molecule. At this stage our results are identical to theirs except for the treatment of electron screening. The binary collision assumption is characteristic of all previous calculations of fast H_2^+ vibrational dissociation. The limitations of this approximation are discussed later in this section.

The final approximation introduces the classical binary collision energy conservation requirement and a heuristic treatment of the correlation between the directions of $\hat{K}$ and $\hat{k}$. We write

$$\left|I(\pm\vec{K},\vec{k})\right|^2 = (2/mk)F(\pm\hat{\vec{K}}\cdot\hat{\vec{k}})\delta(K^2/4m - D_\nu - k^2/m) , \quad (6)$$

where $\delta(\ )$ is the Dirac δ function, D_ν is the dissociation energy for the νth vibrational state, and, at this point, $F(\pm\hat{\vec{K}}\cdot\hat{\vec{k}})$ is restricted only by

$$\int d\Omega(\hat{\vec{k}})F(\pm\hat{\vec{K}}\cdot\hat{\vec{k}}) = 1. \quad (7)$$

Equations (6) and (7) are chosen to guarantee that, aside from the approximate Born treatment of the electron screening, Q_ν is just that given by the classical binary collision theory.[12] The function $F(\hat{\vec{K}}\cdot\hat{\vec{k}})$ determines the relative H_2^+ c.m. angular distribution of dissociation protons. While it has no influence on the total cross section Q_ν, it naturally has an important influence on the laboratory angular distribution of dissociation protons. In initial comparisons between the theory and the experiments of Gibson, Los, and Schopman, it was found that the assumption of isotropy $F(\hat{\vec{K}}\cdot\hat{\vec{k}}) = (4\pi)^{-1}$ gave vibrational dissociation peaks which

were much too broad for large dissociation velocities compared with those shown for example in Fig. 1. This is consistent with Eq. (4) which shows (when χ is replaced by $(2\pi)^{-3/2}\, e^{i\vec{k}\cdot\vec{R}}$) that for large k there should be considerable correlation tending to make $\hat{k}$ and $\hat{K}$ parallel. Accordingly, a heuristic choice of $F(x)$ was made in the form

$$F(x) = (1+2\Gamma)/4\pi[1+\Gamma(1-x)]^2 , \tag{8}$$

with $x \equiv \hat{K}\cdot\hat{k}$

and $$\Gamma = (D_v + k^2/m)/0.0056 . \tag{9}$$

The denominator of Γ was fixed (roughly) by comparing theory and experiment for H_2^+-He collisions. For large Γ, $F(x)$ strongly favors $x=1$; $\Gamma=0$ corresponds to an isotropic c.m. angular distribution. According to the model, strong correlation occurs for low v while little correlation occurs for high v, except if k is large. The influence of $F(x)$ will be illustrated in Sec. III.

From Eqs. (2), (5), and (6), with $\vec{u} = \vec{k}/m$ and $K = 2m(u^2 + D_v/m)^{1/2}$,

$$Q_v = V_0^{-2} \int u^2 du \int d\Omega(\hat{u}) \int_0^{2\pi} d\phi_K |\epsilon_T|^2 \times [1 - \tfrac{1}{2}(1+\tfrac{1}{4}K^2)^{-2}]^2 [F(x)+F(-x)]/u(D_v+mu^2)^2 . \tag{10}$$

We now discuss the formulas for the laboratory-frame angular distributions. Let $\vec{V}_p$ be the dissociation proton laboratory velocity. Then

$$\vec{V}_p = \vec{V}_0 - \vec{K}/(2m) + \vec{u} . \tag{11}$$

Now by Eq. (6), K is a function of u. Moreover, by definition,

$$\vec{K} = \mu(\vec{V}_0 - \vec{V}_n) ,$$

and by energy conservation

$$V_n^2 = V_0^2 - (2/\mu)(D_v + mu^2 + E_T) ,$$

where E_T is the target internal excitation energy. These equations allow one to express the components of $\vec{K}$ perpendicular to and parallel to $\vec{V}_0$ as functions of u. For example, the parallel component of $\vec{K}/(2m)$ is given by

$$[E_T + (1 + 2m/\mu)(D_v + mu^2)]/2mV_0 . \tag{12}$$

With this expression and the corresponding one for the perpendicular component of $\vec{K}/(2m)$, the vector equation (11) describes a transformation from H_2^+ c.m. variables $\vec{u}$, ϕ_K to laboratory variables $\vec{V}_p$, ϕ_K which can be solved for $\vec{u}(\vec{V}_p, \phi_K)$ and for which the Jacobian can be calculated by standard but tedious manipulations. The laboratory differential cross section $dQ_v/(dV_p d\Omega(\hat{V}_p))$ can then be deduced from Eq. (10).

Defining the Jacobian J by $d\vec{V}_p = J\, d\vec{u}$ we obtain

$$dQ_v/(dV_p d\Omega(\hat{V}_p)) = (V_p/V_0)^2 \int d\phi_K J^{-1} |\epsilon_T|^2 \times [1 - \tfrac{1}{2}(1+\tfrac{1}{4}K^2)^{-2}]^2 [F(x) + F(-x)]/u(D_v+mu^2)^2 . \tag{13}$$

The explicit formulas for J, u, and x are too long to present here. The limits on ϕ_K in Eq. (13) are determined by the range of ϕ_K for which Eq. (11) has non-negative solutions for u^2. The quadrature in Eq. (13) was carried out numerically to a relative precision of one part in 10^4.

This section will now be concluded with a brief discussion of the merits and shortcomings of the model. The strong points of the calculation are:

(a) The considerable deflection of the H_2^+ c.m. for vibrational dissociation from states of low v is taken into account in Eq. (11).

(b) Electron screening is allowed for in a reasonable way.

(c) The anisotropy of the c.m. angular distribution is accounted for heuristically in a way which is qualitatively correct. The weakest points in the calculation can be appraised by the arguments of Gerasimenko and Oksyuk.[11] They give conditions for the validity of the use of the sudden approximation and the binary collision approximation upon which their formulation and the classical binary collision theory are based. Following their reasoning, but inserting a factor of 2 on the right-hand side of their equation for $\Delta P\,(\equiv K)$, we find for H_2^+ that the sudden approximation is valid if $V_0 \gg (Z_T e^2/\hbar)^{1/2} \times (D_v/m)^{1/4} \equiv v_1$ and the binary collision approximation is valid if $V_0 \gg (Z_T e^2/R_0)(D_v m)^{-1/2} \equiv v_2$. Here Z_T is the effective target charge and R_0 is the effective internuclear separation. Table I shows representative values of v_1 and v_2 for some extreme cases, Z_T being determined from ϵ_T for an appropriate value of K. For H_2^+ impact energies of 3, 10, and 20.4 keV, V_0 is respectively 0.25, 0.45, and 0.64 a.u. Evidently the criteria are barely satisfied for He and badly violated for Xe in the energy range covered by the experiments. Generally, the binary collision criterion is the least well satisfied. It is the author's belief that the binary collision model overestimates the dissociation cross section.

TABLE I. Values of v_1 and v_2 in a.u. for selected cases.

Target	He	Ne	Ar	Xe
$v_1(v=0)$	0.12	0.27	0.36	0.61
$v_2(v=0)$	0.08	0.38	0.68	2.03
$v_1(v=17)$	0.02	0.04	0.06	0.10
$v_2(v=17)$	0.10	0.29	0.59	1.27

We conclude that while the theory should exhibit the proper qualitative behavior for the dissociation proton angle and velocity distributions, quantitative agreement with experiment cannot be expected. Fortunately, this situation is not entirely devastating since, as will be seen in Sec. III, the angle and velocity distributions from vibrational dissociation turn out to be qualitatively very different from those due to dissociation via transitions to one of the excited electronic states of H_2^+.

III. RESULTS AND DISCUSSION

The general character of the results can be understood by noting that the reciprocal of $u(\vec{V}_p, \phi_K)$ figures in the integrand in Eq. (13). Thus the integrand is singular whenever Eq. (11) admits a solution $u(\vec{V}_p, \phi_K) = 0$ for some ϕ_K. The analysis shows that this occurs for the initial vibrational state ν if and only if

$$V_p \cos\xi - V_0 = -[E_T + (1 + 2m/\mu)D_\nu]/(2mV_0), \quad (14)$$

$$V_p \sin\xi = [D_\nu/m - E_T^2/(4mE_0)]^{1/2}, \quad (15)$$

where $E_0 = mV_0^2$ and ξ is the small angle between $\vec{V}_p$ and $\vec{V}_0$. When Eqs. (14) and (15) are satisfied, the ϕ_K integral in Eq. (13) diverges logarithmically. Thus, ignoring the other factors in Eq. (13) temporarily, the differential cross section has an infinite peak at the single V_p, ξ combination which satisfies Eqs. (14) and (15). The cross section decreases as one moves away from this point in the V_p, ξ plane in any direction.

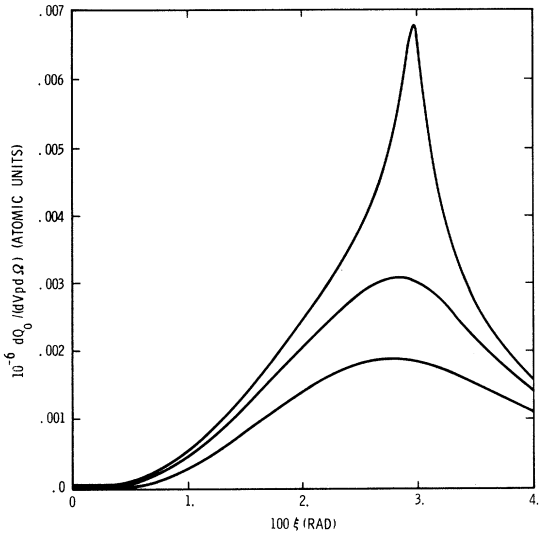

FIG. 2. Proton laboratory angular distribution for vibrational dissociation of 3-keV H_2^+ initially in the ground vibrational level during collisions with He. In order of decreasing magnitude the curves correspond to $\delta \equiv (V_p - V_0)/V_0 = 0.0$, 0.005, and 0.01. Here V_p is the proton velocity and V_0 is the H_2^+ beam velocity. The distributions for $\delta = -0.005$ and $\delta = -0.01$ are very similar to the ones for $\delta = 0.005$ and $\delta = 0.01$. These curves were obtained with an isotropic c.m. angular distribution.

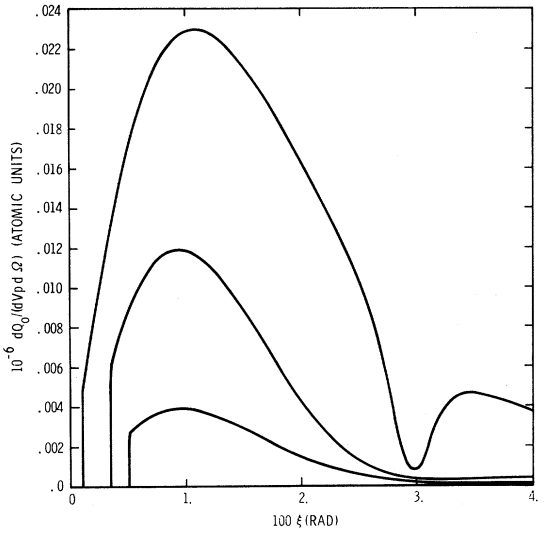

FIG. 3. See Fig. 2. These curves were obtained using the anisotropy factor defined in Eqs. (8) and (9).

This behavior is illustrated in Fig. 2 which shows the differential cross section for $\nu = 0$ plotted versus ξ for 3-keV H_2^+-He collisions with $E_T = 0$ and an isotropic c.m. angular distribution. $[F(x) = (4\pi)^{-1}.]$ The three curves correspond to $(V_p - V_0)/V_0 \equiv \delta = 0.0$, 0.005, and 0.01. The cross section has a sharp peak for $\delta = 0$, since this choice of δ allows Eqs. (14) and (15) to be nearly satisfied at one value of ξ. For $\nu = 0$, the required values of K are always large. Hence the elastic scattering factor $|\epsilon_T|^2$ is nearly equal to the square of the target charge and $[\ ]^2$ in Eq. (13) is close to unity.

The dramatic influence of the anisotropy factor $F(x)$ on this cross section is illustrated in Fig. 3.[13] When ξ is smaller than the value 0.029 7 given by Eqs. (14) and (15), the H_2^+ dissociation must send the proton toward the beam direction to compensate for the transverse H_2^+ c.m. deflection. This tends to make $x \equiv \hat{K} \cdot \hat{u} = 1$ so that by Eq. (8) $F(x) + F(-x)$ is large. As ξ is increased, x decreases through zero to values ~ -1, which apply when ξ is greater than 0.029 7 and the H_2^+ dissociation must send the proton away from the beam direction to reach the detector. With the described increase in ξ, $F(x) + F(-x)$ first decreases to small values and increases again to large ones. This leads to the results shown in Fig. 3.[14]

Similar results are obtained for the case in which one sums over all inelastic transitions in the target,

using closure. In this case, E_T is set equal to the target ionization potential and the target's incoherent scattering factor is used for $|\epsilon_T|^2$. The main difference is that the cross section analogous to that of Fig. 2 has its sharp maximum for $\delta \sim -0.0048$. Screening is unimportant and the influence of $F(x)$ is quite analogous to that shown in Fig. 3.

Some typical results for the high vibrational states are shown in Figs. 4–6. Figure 4 shows the angular distribution for $\delta = 0$ summed over all 20 initial vibrational states using Franck-Condon factors for the vibrational population.[15] The sharp peaks at and to the right of $\xi = 1.9 \times 10^{-4}$ are due to the initial states with $\nu = 19$, 18, 17, and 16. The peak near $\xi = 10^{-5}$ is due to competition in the cross section for $\nu = 19$ between the tendency of u^{-1} to increase the cross section and $|\epsilon_T(K)|^2$ to decrease the cross section as $u \to 0$. For values of δ on either side of zero, the cross sections are smaller and the peaks are less pronounced. The anisotropy factor $F(x)$ has only a small ($\sim 15\%$) quantitative influence on the cross sections for large ν. By contrast, screening plays a large role, as is indicated in Fig. 5 which shows the same cross section computed with the screening factors replaced by the square of the target charge. Without allowance for screening, the initial state $\nu = 19$ dominates everything else. As a final example, Fig. 6 shows the same cross section sum given in Fig. 4, except that this time all inelastic transitions in the He target were summed, with $E_T = 0.9034$. The value of δ is -0.0041 and the sharp peaks correspond to $\nu = 16$ and 15. The broad peak represents contributions from $\nu \geq 17$; for these states the argument of the square root in Eq. (15) is negative. In this case the influences of screening and $F(x)$ are not large.

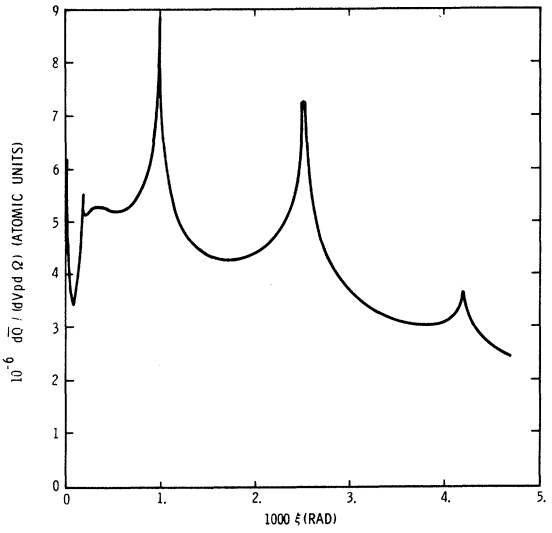

FIG. 4. Proton laboratory angular distribution at $\delta = 0$ for 3-keV H_2^+-He collisions. This cross section $d\bar{Q}/(dV_p d\Omega)$ is the Franck-Condon average of those for all the vibrational states of H_2^+ in its ground electronic state. The target remains in its ground state. Note the change in angular scale.

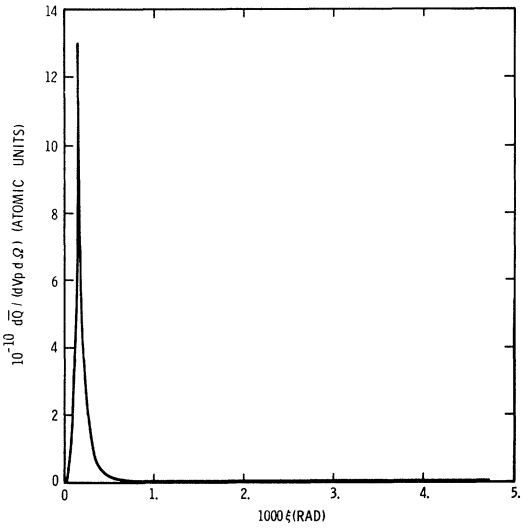

FIG. 5. Same as Fig. 4 except that the electron screening factors were dropped and bare nuclear charges used in the interaction. Note the change in vertical scale.

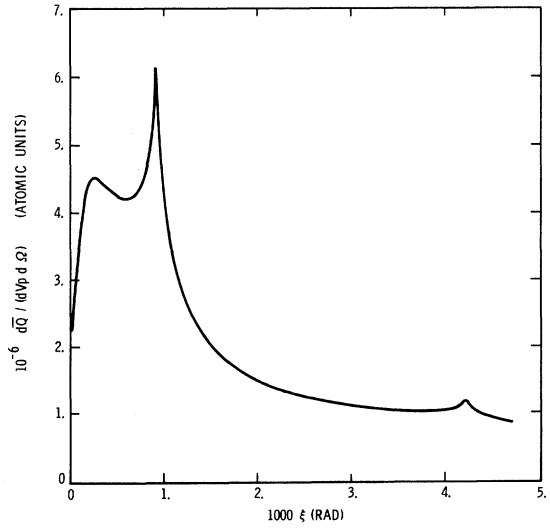

FIG. 6. Same as Fig. 4 except that all inelastic transitions in the He target were summed using closure with $E_T \equiv 0.9034$. Here $\delta = -0.0041$.

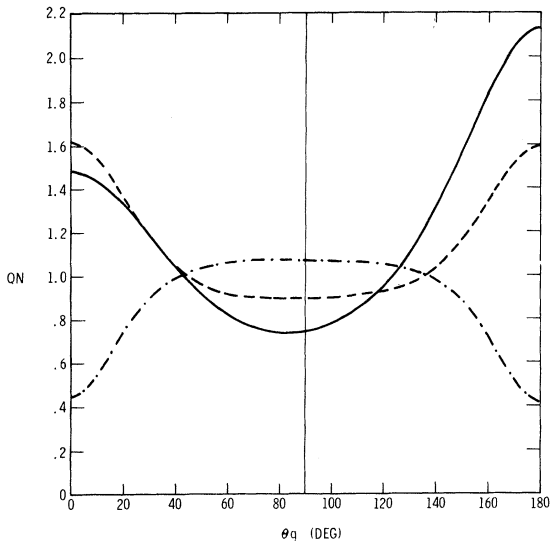

FIG. 7. Apparent H_2^+ c.m. dissociation angular distribution for 3-keV H_2^+-He collisions. The normalization is the same used in Fig. 1. However, θ_g is measured from the forward beam direction. The target remains in its ground state. A Franck-Condon average of initial vibrational states is used. Only the cross section for $2p\sigma_u$ excitation is shown. The solid, dashed, and dot-dashed curves correspond to $R=2.4$, 3.2, and 5.0 as in Fig. 1.

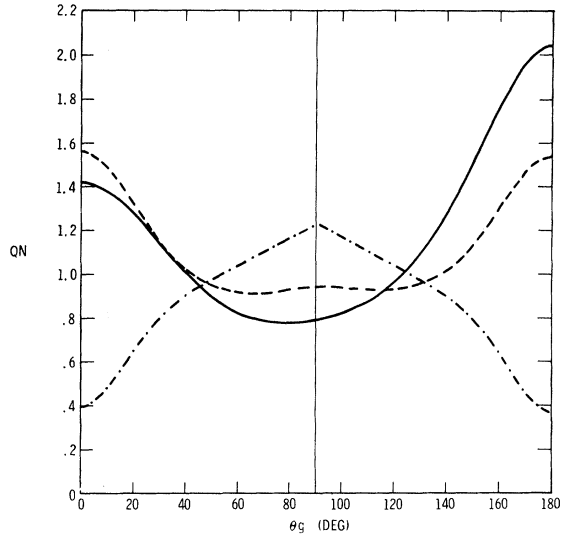

FIG. 9. Same as Fig. 8 except that an isotropic c.m. angular distribution assumed for vibrational dissociation.

Figures 7–10 relate to the experimental data shown in Fig. 1 and were obtained as described below. The target, He, and the impact energy, 3 keV, were chosen with Table I in mind and in order to make $2p\sigma_u$ excitation the only important electronic excitation of H_2^+. Following the procedure in Ref. 1, three H_2^+ c.m. proton velocities u_g were chosen corresponding to the values of R shown in Fig. 1 for the $2p\sigma_u$ state. For each value of u_g and a series of apparent c.m. dissociation angles $0 \leq \theta_g \leq \pi$, laboratory angles ξ and laboratory proton velocities V_p were computed from the relations

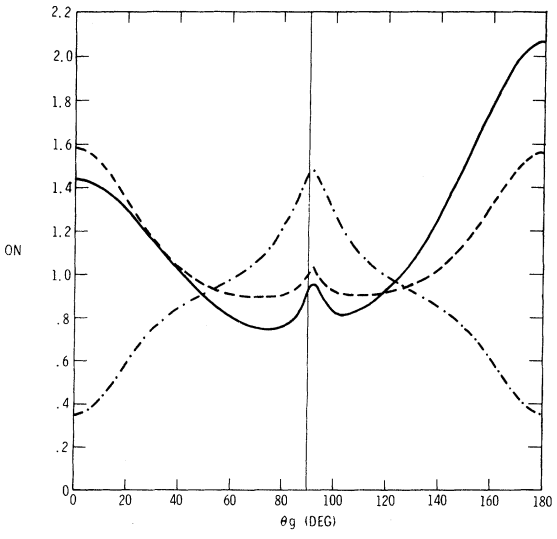

FIG. 8. Same as Fig. 7 except that 0.1 times the computed vibrational dissociation cross section was added to the $2p\sigma_u$ cross section.

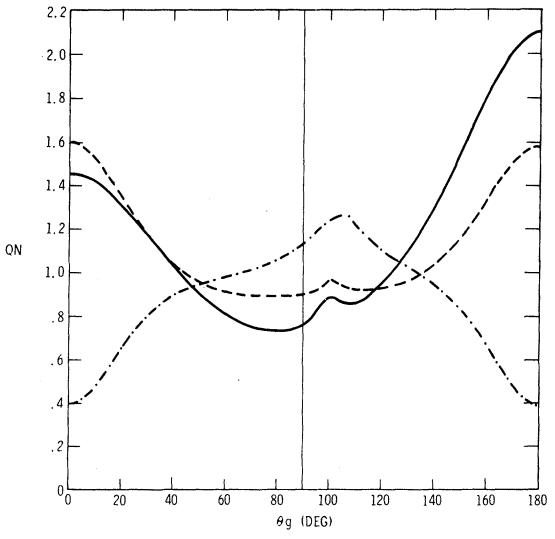

FIG. 10. Same as Fig. 8 except that inelastic transitions in the target were summed using closure and $E_T=0.9034$.

$$V_p \cos\xi = \hat{V}_0 + u_g \cos\theta_g, \quad V_p \sin\xi = u_g \sin\theta_g \quad , \quad (16)$$

which describe the c.m. to laboratory transformation if $\vec{K}$ is neglected in Eq. (11). For each ξ, V_p combination the laboratory $2p\sigma_u$ excitation and vibrational dissociation cross sections were calculated using the results of Ref. 2 and this paper. For the $2p\sigma_u$-state laboratory-frame calculation, the transverse component only of the momentum transferred to the H_2^+ c.m. was neglected in Eq. (11). This led to transformation equations similar to Eqs. (16), except that V_0 was replaced by

$$V_0 - (E_T + D_\nu + mu_g^2)/(2mV_0) \quad .$$

The two laboratory cross sections were added together and multiplied by the Jacobian u_g^2/V_p^2 related to Eq. (16). This defined apparent c.m. cross sections $\sigma(u_g, \theta_g)$ for fixed u_g and variable θ_g. These were then normalized so that

$$\tfrac{1}{2}\int_0^\pi \sin\theta_g \sigma(u_g, \theta_g) d\theta_g = 1$$

and plotted in the figures as QN versus θ_g.[16,17] In Figs. 7–10, θ_g is zero for dissociation in the direction of the H_2^+ beam; it is the complement of ϕ in Fig. 1 so a reflection of Fig. 1 about $\phi = 90°$ is required in the comparison. Fig. 7 shows the $2p\sigma_u$ contribution alone. Figure 8 adds 0.1 times the calculated vibrational dissociation cross section. Figure 9 is similar to Fig. 8 except that an isotropic c.m. vibrational dissociation angular distribution was used [$\Gamma = 0$ in Eq. (8)]. Finally, Fig. 10 adds 0.1 times the vibrational dissociation cross section computed with the regular Γ assuming a closure sum over all inelastic transitions in the He target and using $E_T = 0.9034$. A Franck-Condon distribution was used for the initial vibrational population.

Let us first compare the various theoretical results with each other. From Figs. 7–10, one sees that vibrational dissociation is important around $\theta_g = 90°$, unimportant near $\theta_g = 0°$ or 180°, and most important relative to $2p\sigma_u$ excitation for small u_g. Simultaneous excitation of the target (Fig. 10) causes the peaks to shift to larger values of θ_g.[18] The importance of the anisotropy factor $F(\hat{K}\cdot\hat{k})$ is exhibited in the comparison of Figs. 8 and 9. Clearly, sharp peaks for the larger values of u_g necessitate considerable correlation between $\hat{K}$ and $\hat{k}$. Finally, we mention that screening has very little influence on any of the distributions. This is because in this instance states of low ν ($\nu \sim 4$) dominate the Franck-Condon averaged distributions.

We will now compare theory and experiment, remembering to reflect Fig. 1 about 90°. Qualitative agreement appears best between Figs. 1 and 8 and it is evident that vibrational dissociation is important in Fig. 1. However, from the factor of 0.1 used to weight the computed vibrational dissociation cross section, it is clear that an improved theory would be highly desirable. It is also probable that our choice of $F(x)$ is too anisotropic for the larger values of ν and the smaller values of u_g.

The evidence presented in Figs. 1, 7, and 8 establishes the importance of vibrational dissociation in connection with the interpretation of the experiments described in Ref. 1. The general importance of vibrational dissociation at kV energies was recognized earlier and discussed in qualitative terms by the authors of Refs. 6–8. What is new in the present work is the quantitative application of the classical-impulse binary-collision model to the problem.

It is tempting to use the positions of the peaks in Fig. 1 and Eqs. (14)–(16) to deduce whether and by how much the target is excited on the average during vibrational excitation. This evidently requires accurate experimental measurements which correspond to the initial conditions used in the theory. It also requires more faith in Eqs. (14)–(16) than may be warranted by the approximate nature of the theory. The author's view is that direct experimental studies of the final target state combined with initial H_2^+ vibrational state selection should be carried out.

In conclusion, it may be noted that the $2p\sigma_u$ excitation curves in Figs. 1 and 8 are not in very good quantitative agreement. In particular, the ordering of the curves for $\theta_g = 0°$ is not the same as that for $\phi = 180°$. One should keep in mind that the Born approximation is questionable when $V_0 \sim 0.25$ a.u.

Calculations for other targets, impact energies, initial H_2^+ vibrational populations, etc., can be carried out with the author's programs. This type of information will be supplied by the author, if possible, upon request.

ACKNOWLEDGMENTS

Mrs. Marcella Madsen wrote and checked out the numerous interlocking programs upon which the numerical results depend. J.M. Peek contributed considerably to this paper through his work on Ref. 2 and through many hours of discussion on the physics of the H_2^+ dissociation problem. Helpful discussions or correspondence with G.W. McClure, J. Los, W. Vogler, W. Seibt, R. Caudano, J. Durup, and M. Barat are gratefully acknowledged.

*Work was supported by the U.S. Atomic Energy Commission.

[1]D. K. Gibson, J. Los, and J. Schopman, Physica 40, 385 (1968).

[2]T. A. Green and J. M. Peek, Phys. Rev. 183, 166 (1969).

[3]E. E. Salpeter, Proc. Phys. Soc. (London) A63, 1295 (1950).

[4]D. R. Bates and A. R. Holt, Proc. Phys. Soc. (London) A85, 691 (1965).

[5]K. H. Berkner, S. N. Kaplan, R. V. Pyle, and J. W. Stearns, Phys. Rev. 146, 9 (1966).

[6]W. Vogler and W. Seibt, Z. Physik 210, 337 (1968); B. Meierjohann and W. Seibt, Z. Physik 225, 9 (1969).

[7]J. Durup, P. Fournier, D. Pham, Int. J. Mass Spect. Ion Phys. 2, 311 (1969).

[8]R. Caudano and J. M. Delfosse, J. Phys. B1, 813 (1968).

[9]If the target remains in its ground state, $|\epsilon_T|^2 = [Z_T - F(K)]^2$, where Z_T is the target's nuclear charge and $F(K)$ is its coherent x-ray scattering factor. We use $|\epsilon_T|^2 = S(K)$, where $S(K)$ is the target's incoherent x-ray scattering factor, to describe the closure sum over all inelastic transitions in the target. In this case an approximate effective target excitation energy E_T is introduced into the internal energy conservation equations. This method of using closure is discussed by J. M. Peek, Phys. Rev. 140, A11 (1965); and by T. A. Green and J. M. Peek, *ibid.* 169, 37 (1968). From these papers it can be seen that the use of closure should considerably overestimate the inelastic cross-section sum at the low energies for which experimental data are available. The coherent scattering factor for He is the same used in Ref. 2. The incoherent scattering factor for He was taken from the work of Cromer and Mann, LASL Report No. LA-3689, 1968 (unpublished).

[10]The approximation is equivalent to supposing that the H_2^+ electron screens each proton by spending half its time around it. This screening is important only for the highest values of ν in collisions dominated by values of $K<3$.

[11]V. I. Gerasimenko and Yu D. Oksyuk, Zh. Eksperim. i Teor. Fiz. 48, 499 (1965) [Soviet Phys. JETP 21, 333 (1965)].

[12]Equation (6) can be obtained as the classical limit of the expression for $\int d\Omega\ (\hat{\vec{k}})\,|I(\vec{K},\vec{k})|^2$ used in Ref. 11. In this treatment, the H_2^+ protons are relatively at rest before the collision. An alternative development, which allows for relative proton motion before the collision, is given in Ref. 4. The vibrational dissociation calculations described in Refs. 3–5 and 10 do not allow for electron screening.

[13]The cross sections are zero where Eq. (11) has no solution for $\vec{u}$. They are also zero in Fig. 2 but this is obscured by the choice of scale.

[14]The quantitative aspects of Figs. 2 and 3 cannot be taken too seriously. First of all, the form used for $F(x)$ is a guess. Second, a quantum treatment would blur the sharp relation between u and K, implied by Eq. (6) with the result that the peak in Fig. 2 would be broadened.

[15]The symbol $\overline{Q}$ will be used to denote the Franck-Condon average of the cross sections Q_ν. The Franck-Condon factors were obtained from the work of Rothenberg and Davidson [J. Mol. Spect. 22, 1 (1967)]; and from the work of Villarejo [J. Chem. Phys. 49, 2523 (1968)]. The dissociation energies were obtained from the work of H. Wind, [*ibid.* 43, 2956 (1965)].

[16]In Ref. 1 an additional factor $(1 - u_g \cos\theta_g / V_0)$ is multiplied into the laboratory cross section in the definition of $\sigma(u_g, \theta_g)$. The reader can readily include this small factor in our graphs using $V_0 = 0.245$ and $u_g = 0.011\,15$, $0.007\,750$, and $0.003\,517$.

[17]Because Eqs. (16) are not in general accurate approximations to Eqs. (11), the apparent c.m. cross sections are not equal to the true c.m. cross sections. In particular, the apparent $2p\sigma_u$ c.m. cross section does not possess the symmetry with respect to 90° which is characteristic of the true c.m. cross section (Ref. 2).

[18]The position of the peaks can be obtained roughly from Eqs. (14)–(16). Set $V_p \sin\xi$ equal to $u_g \sin\theta_g$ and solve for D_ν/m using Eq. (15). Use this value in Eq. (14) to obtain $U_g \cos\theta_g = V_p \cos\xi - V_0$ as a function of u_g, θ_g, E_T, and E_0.